ACS OMEGA

http://pubs.acs.org/journal/acsodf

Article

Multi-Domains in a Single Lattice Formed by DNA Self-Assembly

Soojin Jo,[§] Sungjin Lee,[§] Suyoun Park, Anshula Tandon, Thi Bich Ngoc Nguyen, Thi Hong Nhung Vu, Muhammad Tayyab Raza, and Sung Ha Park*

Cite This: *ACS Omega* 2022, 7, 26514−26522

Read Online

ACCESS | Metrics & More | Article Recommendations | Supporting Information

ABSTRACT: Using sequence programmability and the characteristics of self-assembly, DNA has been utilized in the construction of various nanostructures and the placement of specific patterns on lattices. Even though many complex structures and patterns formed by DNA assembly have been reported, the fabrication of multi-domain patterns in a single lattice has rarely been discussed. Multi-domains possessing specifically designed patterns in a single lattice provide the possibility to generate multiple patterns that enhance the pattern density in a given single lattice. Here, we introduce boundaries to construct double- and quadruple-domains with specific patterns in a single lattice and verify them with atomic force microscopy. ON, OFF, and ST (stripe) patterns on a lattice are made of DNA tiles with hairpins (ON), without hairpins (OFF), and alternating DNA tiles without and with hairpins (formed as a stripe, ST). For double- and quadruple-domain lattices, linear and cross boundaries were designed to fabricate two (e.g., ON and OFF, ON and ST, and OFF and ST) and four (OFF, ST, OFF, and ON) different types of patterns in single lattices, respectively. In double-domain lattices, each linear boundary is placed between two different domains. Similarly, four linear boundaries connected with a seed tile (i.e., a cross boundary) can separate four domains in a single lattice in quadruple-domain lattices. Due to the presence of boundaries, the pattern growth directions are different in each domain. The experimentally obtained multi-domain patterns agree well with our design. Lastly, we propose the possibility of the construction of a hexadomain lattice through the mapping from hexagonal to square grids converted by using an axial coordinate system. By proposing a hexadomain lattice design, we anticipate the possibility to extend to higher numbers of multi-domains in a single lattice, thereby further increasing the information density in a given lattice.

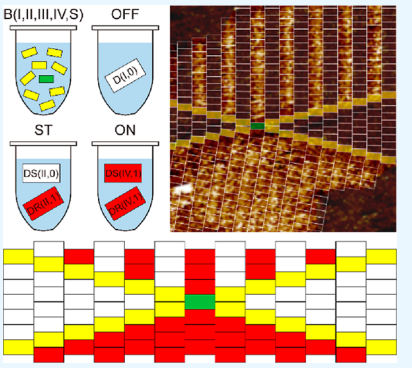

INTRODUCTION

Since the discovery of DNA structures, researchers have studied DNA molecules to understand their functionalities in the fields of biology, medicine, and genetics. DNA molecules possess intrinsic characteristics that are interesting not only in biological sciences, such as its genetic materials, complementarity of base pairs, and well-specified interactions with biological molecules, but also in physical engineering, such as its double helical structure, UV absorption, poor conductivity, and thermal stability.[1] In addition, DNA is considered to be one of the most promising building materials because of the programmability of its base sequences, its high stability compared to other biomolecules, and the characteristics of bottom-up self-assembly.[2−7] Consequently, structural DNA nanotechnology, which provides ways to construct various dimensional nanostructures made of DNA, has made impressive gains over the past 40 years.

DNA nanotechnology encompasses the fabrication of DNA nanostructures, the demonstration of DNA algorithms, the construction of devices and sensors made of DNA, and data storage in DNA.[8] Diverse nanostructures made of DNA tiles and DNA strands without and with long scaffold virus genomes have been reported.[9−21] DNA logic gates can also be constructed by using the implementation of bit information into DNA sequences.[22−28] By embedding functional nanomaterials into DNA molecules, it is feasible to construct a variety of physical devices and biological/chemical sensors.[29−32] One of the promising practical DNA applications in physical engineering is to construct a data storage apparatus that might enhance the capability of data storage in the near future.[33−35]

Among the many ways to construct DNA nanostructures, tile-based DNA assembly possesses many advantages, such as size controllability, structural rigidity, the ease of designing binding domains and shapes, and the capacity to embed secondary structures.[36] To verify the geometry and binding domain of designed DNA tiles, DNA lattices, which are mostly single crystal structures, have to be fabricated by using a standard annealing method. DNA tiles with secondary structures (e.g., duplex hairpins and biotinylated bases) can generate a certain pattern on a single lattice formed by a binding domain design. Although tile-based DNA assembly is

Received: April 25, 2022
Accepted: July 7, 2022
Published: July 19, 2022

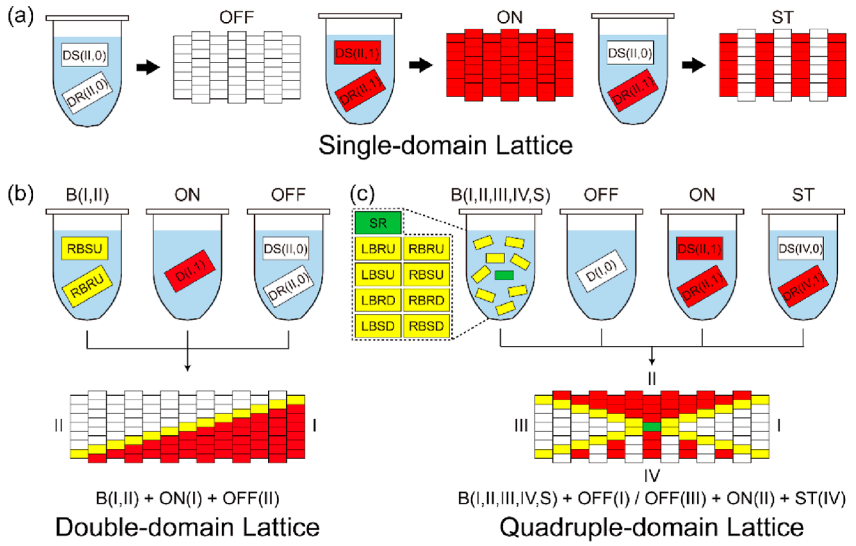

Figure 1. Schematic representation of the fabrication of single-, double-, and quadruple-domains in a single lattice. (a) Fabrication of a single-domain lattice with either OFF, ON, or ST pattern. (b) Fabrication of a double-domain lattice with ON and OFF patterns separated by a linear boundary. A double-domain lattice [that is, B(I,II) + ON(I) + OFF(II)] comprises the linear boundary B(I,II), ON(I), and OFF(II). B(I,II) [OFF(II)] is formed by RBRU and RBSU [DR(II,0) and DS(II,0)]. (c) Fabrication of a quadruple-domain lattice with ON, OFF, and ST patterns separated by a cross boundary. A quadruple-domain lattice [that is, B(I,II,III,IV,S) + OFF(I)/OFF(III) + ON(II) + ST(IV)] consists of OFF(I), ON(II), OFF(III), and ST(IV) in each quadrant separated by B(I,II,III,IV,S).

able to generate complex shapes and patterns based on specifically designed binding domains, the fabrication of multi-domain patterns in a single lattice has seldom been demonstrated compared to the number of examples of single patterns in a single lattice because of the complexity of multi-domain design and associated experimental difficulties.[23−26] Multi-domains in a single lattice provide the possibility to generate multiple patterns through designed DNA tiles, thereby increasing the pattern density in a given single lattice.

In this study, we conceived boundaries to fabricate double- and quadruple-domains in a single lattice by using DNA tiles. In single-domain lattices, we considered three patterns: a plane lattice made of DNA tiles without hairpins (OFF), a lattice made of DNA tiles with hairpins (ON), and a lattice with an alternating line-like pattern (similar to stripes) formed by DNA tiles without and with hairpins (ST). For double- and quadruple-domain lattices, linear and cross boundaries were introduced to fabricate two (e.g., ON and OFF, ON and ST, and OFF and ST) and four (e.g., OFF, ST, OFF, and ON) different types of patterns in single lattices, respectively. To verify the formation of the patterns on the lattices, atomic force microscopy (AFM) was used. Lastly, we proposed the possibility of the construction of a hexadomain lattice through the mapping from hexagonal to square grids converted by using an axial coordinate system.

RESULTS AND DISCUSSION

Design Schemes of Single-, Double-, and Quadruple-Domain Lattices. A schematic representation of the fabrication of a single-domain lattice is shown in Figure 1a. A single lattice comprises two different types of rectangular building blocks (R and S) to generate various patterns such as OFF, ON, and ST. A lattice made of R and S blocks possessing 0-bit (1-bit) information marked as white (red) forms an OFF (ON) pattern. Similarly, a ST pattern can be generated by an alternating line-like pattern using R and S blocks possessing 1- and 0-bit information, respectively. Consequently, single-domain OFF(I) and ON(I) [OFF(III) and ON(III)] lattices in a domain I [domain III] are constructed by using building blocks of D(I,0) and D(I,1) [D(III,0) and D(III,1)], respectively. Here, D, I, III, and 0, 1 stand for DX, domains I, III, and 0-bit, 1-bit possessing blocks, respectively. Interestingly, although tile names are different, D(I,0) and D(III,0) [D(I,1) and D(III,1)] are identical and have same sticky-ends. Similarly, single-domain OFF(II), ON(II), and ST(II) lattices in a domain II are constructed by using building blocks of DR(II,0) and DS(II,0), DR(II,1) and DS(II,1), and DR(II,1) and DS(II,0), respectively.

By using building blocks of single-domain lattices, we can demonstrate multi-domain patterns in a single lattice by introducing specifically designed boundaries. Figure 1b displays the fabrication procedure of a double-domain lattice with ON and OFF patterns separated by a linear boundary (indicated with yellow), which is named B(I,II) + ON(I) + OFF(II). It comprises ON(I), OFF(II), and the linear boundary B(I,II). Here, B(I,II) [OFF(II)] is formed by RBRU and RBSU [DR(II,0) and DS(II,0)]. The Roman numeral in the name of the building block indicates the corresponding quadrant. Figure 1c shows the fabrication of a quadruple-domain lattice with ON, OFF, and ST patterns separated by a cross boundary (indicated with yellow for linear boundaries and green for seed), which is named B(I,II,III,IV,S) + OFF(I)/OFF(III) + ON(II) + ST(IV). It consists of OFF(I), ON(II), OFF(III), and ST(IV) in each quadrant separated by a cross boundary B(I,II,III,IV,S). B(I,II,III,IV,S) is fabricated by using nine building blocks (SR, LBRU, LBSU, LBRD, LBSD, RBRU, RBSU, RBRD, and RBSD). Tile names include the position, type, and growth direction of the boundary. For example, LBSD is placed in the left-side boundary with S type and has a diagonally downward growth direction, whereas RBRU is placed on the right-side boundary with R type and has a diagonally upward growth direction. The seed building block (SR) connects four linear boundaries. Similarly, ON(II) [ST(IV)] is constructed by using DR(II,1)

https://doi.org/10.1021/acsomega.2c02556
ACS Omega 2022, 7, 26514−26522

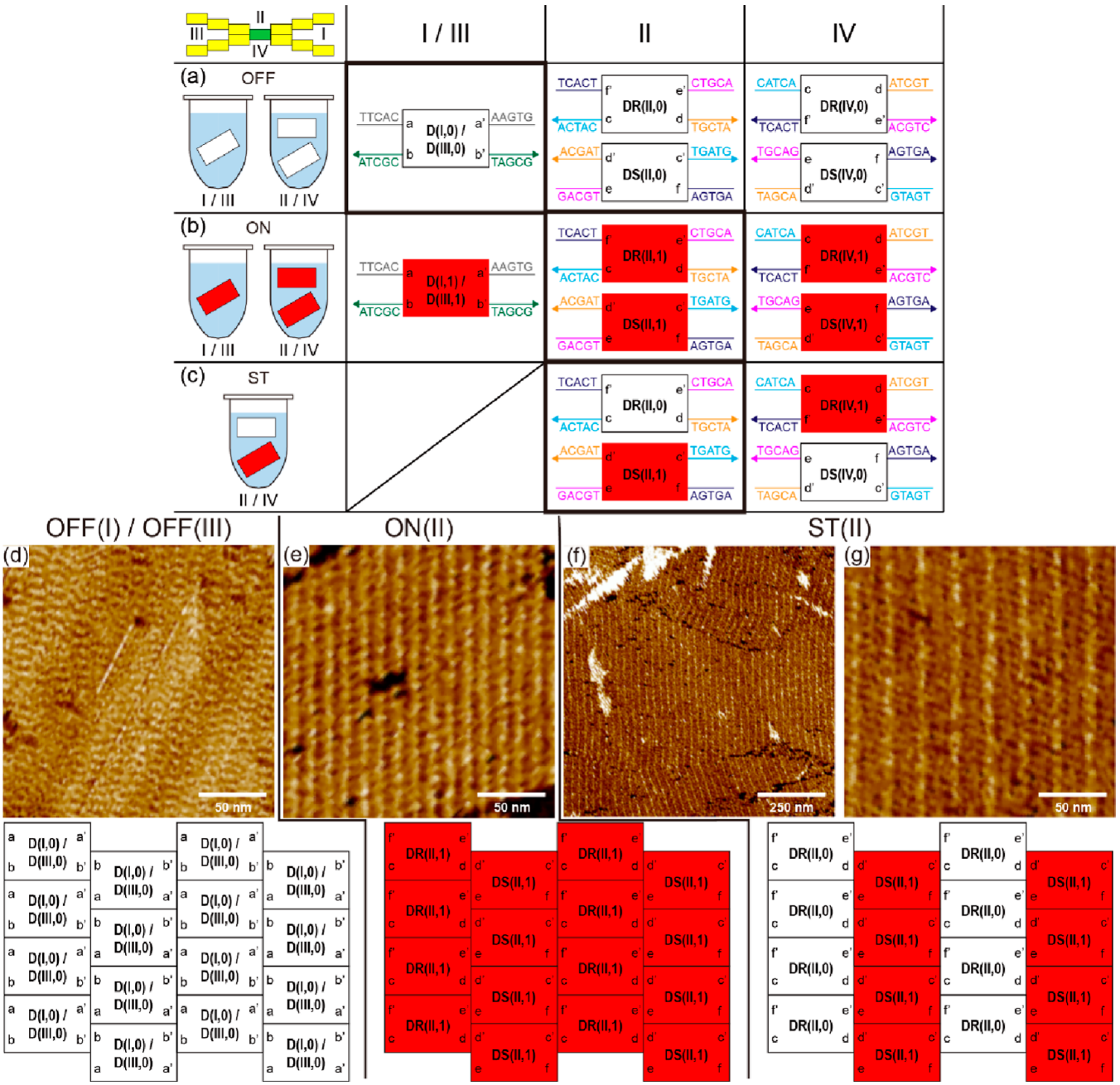

Figure 2. Binding domain design of unit DX tiles for OFF, ON, and ST lattices and their representative AFM images. (a–c) Sticky end design of unit DX tiles in each quadrant for the construction of OFF, ON, and ST lattices. In domains II and IV, we specified R and S types of DX tiles that indicate 5′ → 3′ and 3′ → 5′ directionalities in their stands. In the case of domains I and III, a single unit DX tile used in the OFF (ON) lattice is required and served as both R and S types due to the specific binding domain scheme. To visualize patterns, unit DX tiles were designed without (0) and with (1) protruding DNA hairpins marked as white and red, respectively. Prime and non-prime sticky ends with the same name are complementary to each other (e.g., a and a′). (d–g) Representative AFM images and corresponding lattice schematics (size of 4 × 4) of DX DNA lattices with the OFF pattern in domain I or III [that is, OFF(I)/OFF(III)], the ON pattern in domain II [that is, ON(II)], and the ST pattern in domain II [that is, ST(II)]. Scan sizes in all AFM images are 200 × 200 nm^2 except (f), which is 1 × 1 μm^2.

and DS(II,1) [DR(IV,1) and DS(IV,0)]. Although a lattice with an OFF or ON pattern comprises two different building blocks in domains II and IV, a single unit building block [that is, D(I,0) for OFF and D(I,1) for ON] is required in the case of domains I and III.

Design and Fabrication of Single-Domain DNA Lattices. Figure 2a–c shows the sticky end design of a unit of DNA double-crossover (DX) tiles in each quadrant for the fabrication of DNA lattices with OFF, ON, and ST patterns.[3,17] A rectangular shaped DX tile (with length and width of 12.6 and 6 nm, respectively) comprises four DNA strands and is used in the construction of 1D and 2D lattices.[10−19] Each domain is represented by Roman numerals (I, II, III, and IV). In domains II and IV, we have specified R and S types of DX tiles that indicate 5′ → 3′ and 3′ → 5′ directionalities in their strands, respectively.[25−28] In the case of domains I and III, a single unit DX tile used in an OFF [D(I,0) is identical to D(III,0)] or ON [D(I,1) is identical to D(III,1)] lattice is

https://doi.org/10.1021/acsomega.2c02556
ACS Omega 2022, 7, 26514−26522

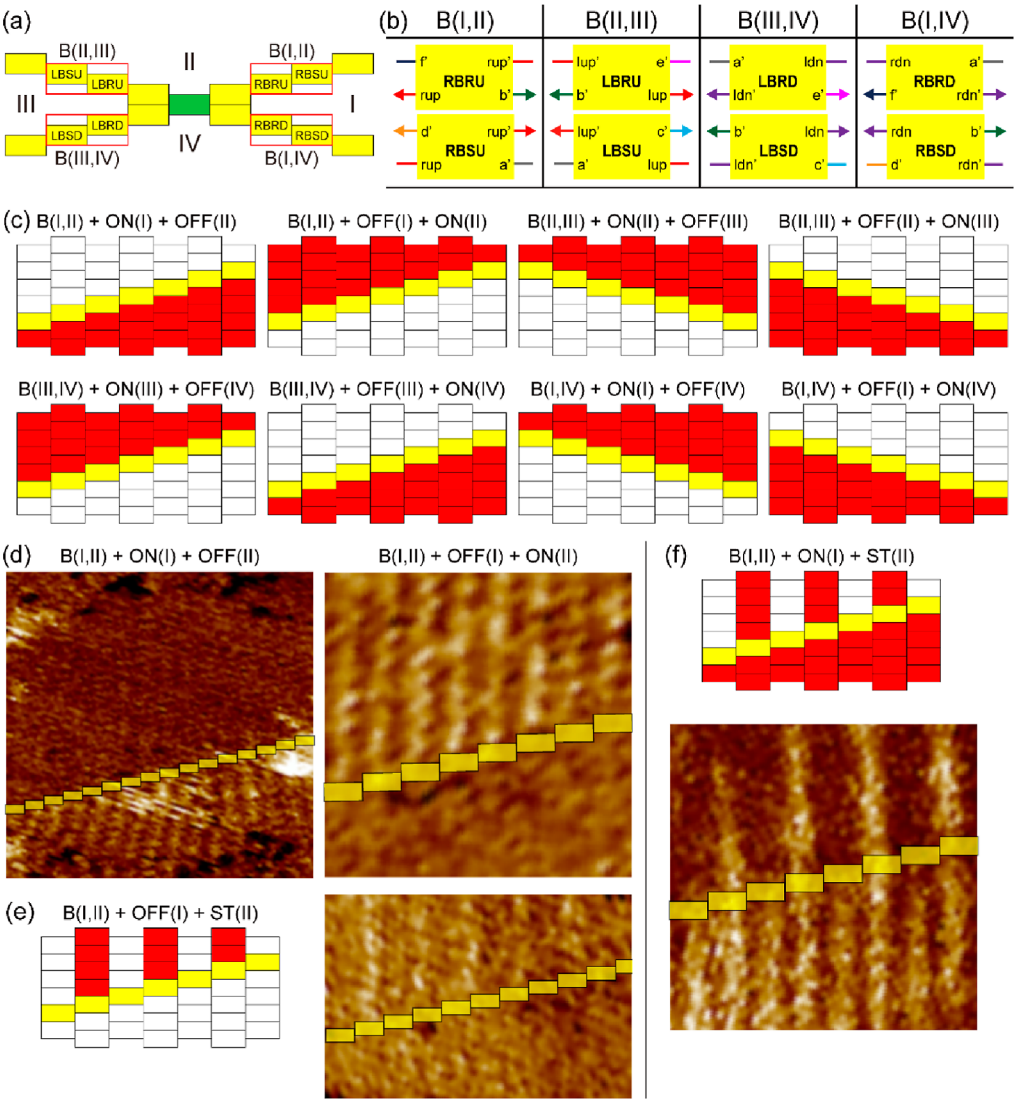

Figure 3. Binding domain design of unit DX tiles for four different linear boundaries, schematics, and their representative AFM images of double-domain lattices. (a) Four kinds of linear boundaries, B(I,II), B(II,III), B(III,IV), and B(I,IV). Each boundary is placed between two different domains. (b) Sticky end design of unit DX tiles for each boundary. Tile names include the position, polarity, and growth direction of the boundary. (c) Double-domain lattices with ON and OFF patterns. Individual DX tiles for the boundary, ON, and OFF are shown, as yellow, red, and white, respectively. Eight possible double-domain lattices with ON and OFF patterns are displayed. (d) Two representative AFM images of the double-domain lattices B(I,II) + ON(I) + OFF(II) and B(I,II) + OFF(I) + ON(II). To clarify boundaries, overlaid guidelines with yellow boxes (corresponding to RBRU and RBSU) were added. Scan sizes on left and right are 200 × 200 and 100 × 100 nm^2, respectively. (e) A representative AFM image of B(I,II) + OFF(I) + ST(II) with a scan size of 150 × 100 nm^2. (f) A representative AFM image of B(I,II) + ON(I) + ST(II) with a scan size of 100 × 100 nm^2.

required and serves as both R and S types due to the specific sticky end design. Here, non-prime (input) and prime (output) sticky ends with the same name and color are complementary (e.g., b and b′). This means that pattern growth directions are different in each domain. Pattern growth directions are left to right, bottom to up, right to left, and up to bottom in domains I, II, III, and IV, respectively. To visualize patterns, unit DX tiles are decorated without (possessing 0-bit) and with (possessing 1-bit) protruding DNA hairpins marked as white and red, respectively (see Supporting Information, Figures S1 and S2, and Tables S1−S3 for DNA base sequences). For example, D(III,0), DR(II,1), and DS(IV,0) tiles indicate a DX tile without DNA hairpins formed in the third quadrant for an OFF lattice, a DX tile with DNA hairpins formed in the second quadrant for ON, and a DX tile without DNA hairpins formed in the fourth quadrant for ST. Three patterns on DNA lattices using two DX tiles were fabricated in domains II and IV. For example, ON(II) and ST(IV) were fabricated by using DR(II,1) and DS(II,1) for domain II and DR(IV,1) and DS(IV,0) for domain IV.

Representative AFM images of DX DNA lattices with an OFF pattern in domain I or III [that is, OFF(I)/OFF(III)], an ON pattern in domain II [that is, ON(II)], and an ST pattern in domain II [that is, ST(II)] are shown in Figure 2d−g. Both ON (Figure 2e) and ST (Figure 2g) lattices show line-like patterns, but the interval between lines in the ST lattice is twice that in the ON lattice, which agrees well with our design.

Design and Fabrication of Double-Domain DNA Lattices. A binding domain design of unit DX tiles for linear boundaries to construct double-domain DNA lattices is shown

https://doi.org/10.1021/acsomega.2c02556
ACS Omega 2022, 7, 26514−26522

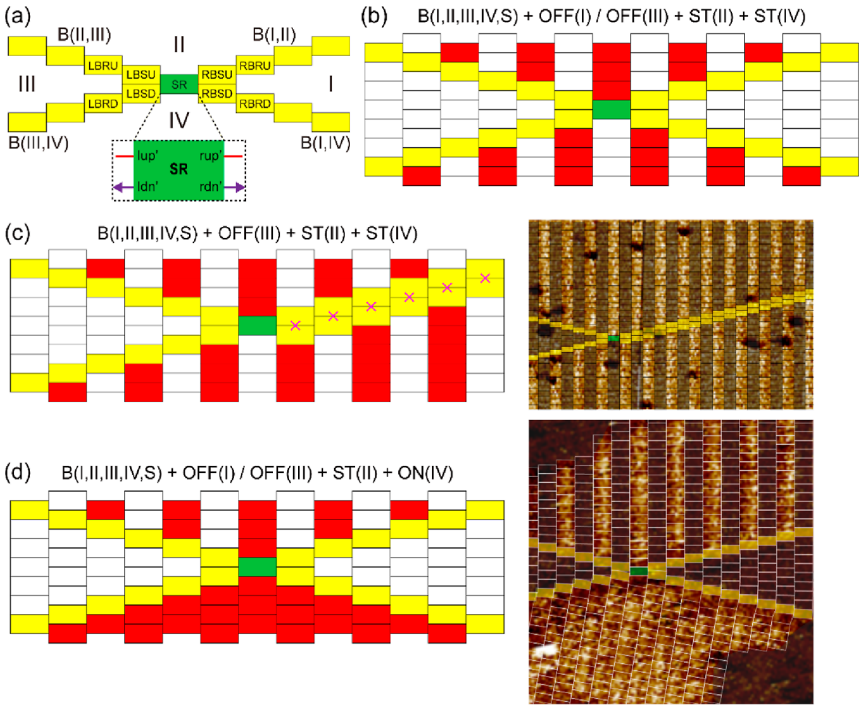

Figure 4. Binding domain design of unit DX tiles for a cross boundary, schematics, and their representative AFM images of quadruple-domain lattices. (a) Schematic of a cross boundary B(I,II,III,IV,S) comprising four linear boundaries [that is, B(I,II), B(II,III), B(III,IV), and B(I,IV)] and a single seed tile (SR). (b) Schematic of a quadruple-domain lattice with OFF patterns in domain I/III and ST patterns in domains II and IV named as B(I,II,III,IV,S) + OFF(I)/OFF(III) + ST(II) + ST(IV). (c) Representative AFM image of B(I,II,III,IV,S) + OFF(III) + ST(II) + ST(IV) with its corresponding schematic representation. For clarity, the overlaid guidelines (green, yellow, and gray for seed, boundary, and DX tiles without hairpins, respectively) are provided. Scan size is 300 × 200 nm^2. Due to the non-specific binding between B(I,II) and B(I,IV) marked with magenta crosses, an unexpected triple-domain lattice is observable. (d) Schematic and a corresponding AFM image of a quadruple-domain lattice B(I,II,III,IV,S) + OFF(I)/OFF(III) + ST(II) + ON(IV) with overlaid guidelines (scan size of 200 × 200 nm^2).

in Figure 3a,b. Four kinds of linear boundaries [B(I,II), B(II,III), B(III,IV), and B(I,IV)] are formed by using two DX tiles, such as RBRU and RBSU for B(I,II), LBRU and LBSU for B(II,III), LBRD and LBSD for B(III,IV), and RBRD and RBSD for B(I,IV) (see Supporting Information, Figures S1 and S2 and Tables S1−S3 for DNA base sequences). Each boundary is placed between two different domains. For example, a linear boundary B(II,III) separate domains II and III. Figure 3b shows detailed sticky end information of the unit DX tiles for each boundary. Tile names include the position [left-side boundary (LB) or right-side boundary (RB)], polarity (R or S type), and growth direction [upward (U) or downward (D)] of the boundary. For example, RBRU in B(I,II) is placed in the right-side boundary with R type polarity and has a diagonally upward growth direction. Each tile is incorporated into binding information for pattern and boundary with specific colors. A set of sticky ends (lup and lup′, ldn and ldn′, rup and rup′, and rdn and rdn′) in each boundary tile has nine nucleotides, which enhance the binding affinity between two boundary tiles and the structural stability of the boundary. Consequently, two DX tiles in each boundary alternatively bind each other due to their polarities (which come from the 3.5 full-turn-length of the DX tile). Other sticky ends (a′, b′, c′, d′, e′, and f′) have five nucleotides as binding information for patterns.

Schematics and representative AFM images of double-domain lattices with ON and OFF patterns are shown in Figure 3c,d. Individual DX tiles for boundary, ON, and OFF are represented as yellow, red, and white, respectively. Eight possible double-domain lattices with ON and OFF patterns are displayed. One of the lattices with the ON pattern in domain I and the OFF pattern in domain II grown from a linear B(I,II) boundary is named as B(I,II) + ON(I) + OFF(II). Among the eight possible lattices, representative AFM images of the double-domain lattices B(I,II) + ON(I) + OFF(II) and B(I,II) + OFF(I) + ON(II) are displayed in Figure 3d. To clarify the boundaries, the overlaid guidelines with yellow boxes (which correspond to RBRU and RBSU) are embedded (Figure S3 in the Supporting Information shows AFM images without overlaid guidelines). As expected, the length between lines on the ON pattern and the length of RBRU (or RBSU) are almost the same, which indicates the appropriate formation of double domains in a single lattice. Similarly, we also have constructed a double-domain lattice with OFF (ON) in domain I and ST in domain II using a linear boundary {that is, B(I,II) + OFF(I) [ON(I)] + ST(II)} (Figure 3e,f). Based on the AFM images, the intervals between lines on the ST pattern are doubled compared to the ON pattern, as we designed.

Design and Fabrication of Quadruple-Domain DNA Lattices. Figure 4 displays the binding domain design of unit DX tiles for a cross boundary, schematics, and representative AFM images of quadruple-domain lattices. A cross boundary B(I,II,III,IV,S) comprises four linear boundaries [that is, B(I,II), B(II,III), B(III,IV), and B(I,IV)] and a single seed tile (SR). SR connects four linear boundaries that allow it to generate four different patterns in a single lattice.

Figure 4b shows a schematic of a quadruple-domain lattice with OFF patterns in domains I and III and ST patterns in domains II and IV named as B(I,II,III,IV,S) + OFF(I)/OFF(III) + ST(II) + ST(IV). Only a single DX tile, D(I,0) [=

https://doi.org/10.1021/acsomega.2c02556
ACS Omega 2022, 7, 26514−26522

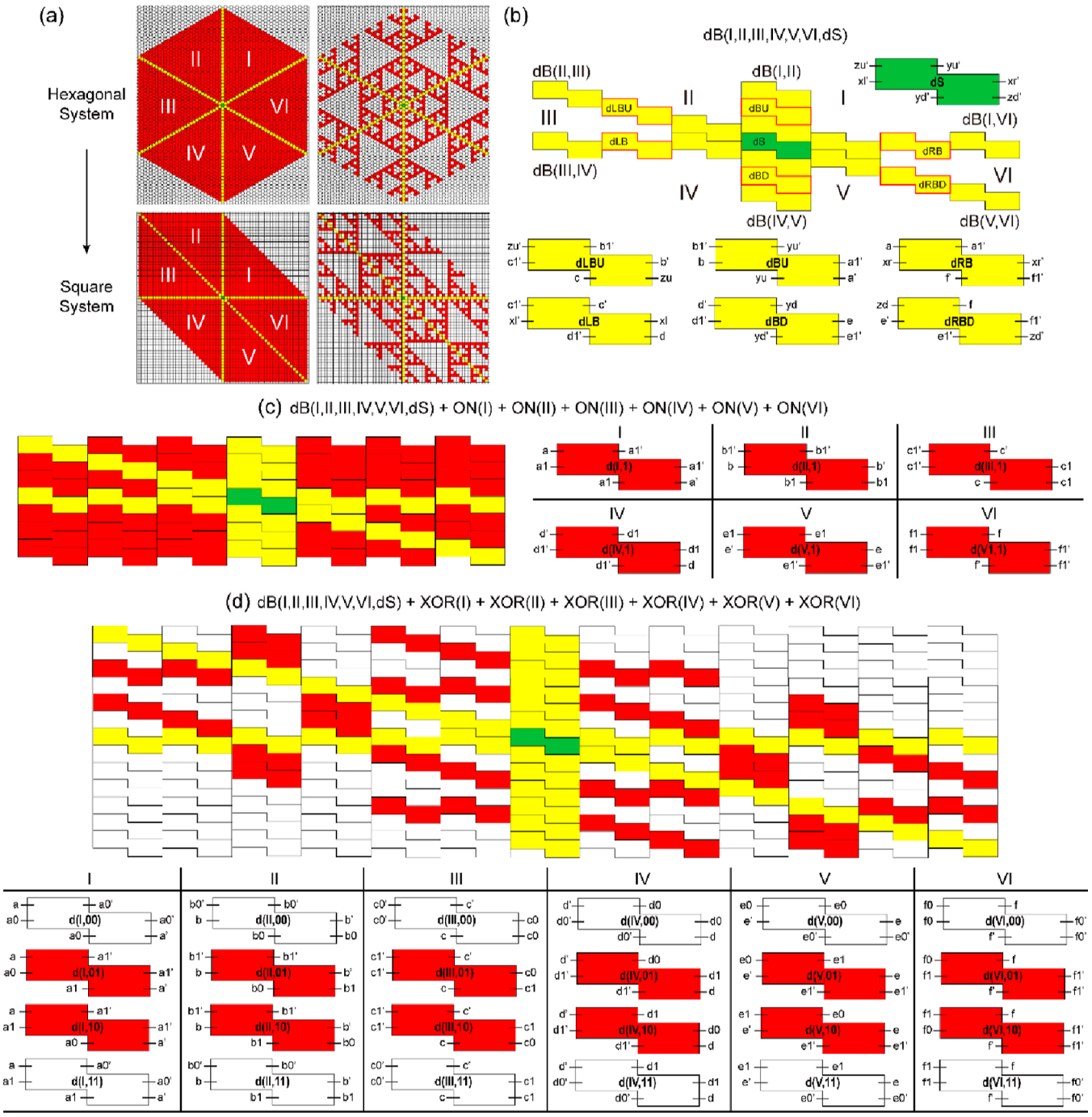

Figure 5. Design of hexadomain lattices with ON and XOR patterns by using double DX (dDX) tiles. (a) Mapping from hexagonal to square grids converted by using an axial coordinate system for ON and XOR hexadomain lattices. (b) Design of a hexadomain boundary by using unit dDX tiles. The schematic of a hexadomain boundary dB(I,II,III,IV,V,VI,dS) comprises six linear boundaries [dB(I,II), dB(II,III), dB(III,IV), dB(IV,V), dB(V,VI), and dB(I,VI)] and a single seed tile (dS). Seed and boundary dDX tiles are colored green and yellow, respectively. (c) Schematics and unit dDX tile design of a hexadomain lattice of dB(I,II,III,IV,V,VI,dS) + ON(I) + ON(II) + ON(III) + ON(IV) + ON(V) + ON(VI). In each domain, a single unit dDX tile is needed [d(I,1), d(II,1), d(III,1), d(IV,1), d(V,1), or d(VI,1)], which is colored as red. (d) Schematics and unit dDX tile design of a hexadomain lattice of dB(I,II,III,IV,V,VI,dS) + XOR(I) + XOR(II) + XOR(III) + XOR(IV) + XOR(V) + XOR(VI). In each domain, four unit dDX tiles that possess output information of either 0-bit (white) or 1-bit (red) are required.

D(III,0)], is required for OFF(I) and OFF(III) with a cross boundary. For ST patterns, unit DX tiles of DR(II,1), DS(II,0) for ST(II) and DR(IV,0), DS(IV,1) for ST(IV) are required. Because of the presence of hairpins in the R type of the DX tile in domain II [DR(II,1)] and the S type of the DX tile in domain IV [DS(IV,1)], alternating stripes in domains II and IV are formed. Interestingly, we obtain an unexpected triple-domain lattice (although such lattices are rarely observed), B(I,II,III,IV,S) + OFF(III) + ST(II) + ST(IV), instead of a quadruple-domain lattice. An AFM image of the triple-domain lattice with its corresponding schematic representation is shown in Figure 4c. For clarity, the overlaid guidelines (green, yellow, and gray for seed, boundary, and DX tiles without hairpins, respectively) are provided. The triple-domain lattice

https://doi.org/10.1021/acsomega.2c02556
ACS Omega 2022, 7, 26514−26522

might occur due to the flexibility of the boundary and nonspecific binding between boundaries. One of the quadruple-domain lattices with OFF in domain I/III, ST in domain II, and ON in domain IV [B(I,II,III,IV,S) + OFF(I)/OFF(III) + ST(II) + ON(IV)] is shown in Figure 4d (Figure S4 in the Supporting Information shows AFM images without overlaid guidelines). The AFM image reveals patterns in each domain separated by a cross boundary. Additionally, the intervals between neighboring lines on ST and ON patterns are noticeable, as designed. A distortion of a quadruple-domain lattice was observed. This might be due to the flexibility of the linear boundaries, assembly flaw during formation of lattices, and the interaction between DNA samples and the mica substrate.

Design Schemes of Hexa-Domain Lattices by Using Double DX Tiles. In addition, we proposed design schemes for hexadomain lattices by using rectangular shaped unit building blocks. We used mapping from hexagonal to square grids converted by using an axial coordinate system. Figure 5a shows hexadomain lattices with ON and XOR patterns in hexagonal and square systems. Although it might be possible to design unit building blocks with six binding domains (e.g., a honeycomb shaped building block), double-rectangular shaped building blocks such as double DX (dDX) tiles could also provide six binding domains.[37] To use dDX tiles, mapping from hexagonal to square systems had to be conducted. Among the various coordinate systems in a hexagonal grid, such as the offset, cube, doubled, and axial coordinate systems, the commonly used axial coordinate system was adapted.[38,39] Cells in each domain followed a one-to-one correspondence between hexagonal and square systems. Interestingly, the square system with hexadomains showed two different angles between axes, 90° for domains I and IV and 45° for II, III, V, and VI.

Figure 5b shows a design scheme of a hexadomain boundary using unit dDX tiles. A hexadomain boundary dB-(I,II,III,IV,V,VI,dS) comprises six linear boundaries [dB(I,II), dB(II,III), dB(III,IV), dB(IV,V), dB(V,VI), and dB(I,VI)] and a single seed tile (dS). Seed and boundary dDX tiles are colored green and yellow, respectively. Consequently, dB-(I,II,III,IV,V,VI,dS) is formed by using dBU, dLBU, dLB, dBD, dRBD, and dRB for boundaries, and dS for seed. Here, non-prime and prime sticky ends with the same name are complementary to each other.

Figure 5c,d shows schematics and the unit dDX tile design of hexadomain lattices with ON and XOR patterns separated by dB(I,II,III,IV,V,VI,dS). For a hexadomain ON lattice, a single unit dDX tile in each domain is needed [that is, d(I,1), d(II,1), d(III,1), d(IV,1), d(V,1), and d(VI,1)]. For example, d(II,1) indicates a unit dDX tile used in domain II carrying the ON (1-bit) information. Similarly, for a hexadomain XOR lattice, four unit dDX tiles in each domain that possess output information of either 0-bit (white) or 1-bit (red) are required. For example, d(I,00) with white [d(III,10) with red] indicates a unit dDX tile used in domain I with 2-input of 00 and 1-output of 0 [unit dDX tile used in domain III with 2-input of 10 and 1-output of 1]. Outputs are determined by an XOR logic operation that gives triangle-embedded fractal patterns on lattices.

CONCLUSIONS

In conclusion, we designed and fabricated single-, double-, and quadruple-domain lattices by introducing linear and cross boundaries. Linear or cross boundaries were used to construct double- or quadruple-domain lattices with two or four, respectively, different types of patterns (of ON, OFF, and ST). Because the boundaries served as separators between domains and templates for pattern growth, it was possible to generate multi-domain lattices and enhance their formations. We also suggested the feasibility of constructing a lattice with six different domains by using a hexadomain boundary through the mapping from hexagonal to square systems. Therefore, our method enables the enhancement of pattern density (higher than quadruple) in a specific single lattice.

METHODS

Fabrication of Single-, Double-, and Quadruple-Domain DNA Lattices. Standard desalt purified synthetic oligonucleotides were purchased from Integrated DNA Technologies (IA, USA). Single-domain DNA lattices and double- and quadruple-domain DNA lattices were obtained by using the two-step and three-step annealing methods, respectively. Individual tiles were formed by mixing a stoichiometric quantity of each DNA strand in a 1× TAE/Mg^{2+} buffer (trisacetate-EDTA: 40 mM Tris, 1 mM EDTA (pH 8.0), 12.5 mM magnesium acetate). In the first annealing step, the test tubes for individual tiles (including seed, boundary, and unit tiles for patterns) were placed in a Styrofoam box with 2 L of boiling water, followed by slow cooling from 95 to 25 °C to facilitate the hybridization process.[3,17] The final tile concentration in each test tube was 1 μM.

For a single-domain DNA lattice, equal amounts of annealed individual tiles of a given pattern were mixed in a new test tube. For example, 5 μL of DR(II,0) and DS(II,1) were added to 40 μL of 1× TAE/Mg^{2+} buffer for ST(II). For OFF(I), 5 μL of D(I,0) without the D(I,0)-4 strand [comprising D(I,0)-1, CB-2, and CB-3 strands] and 5 μL of 1 μM D(I,0)-4 were added to 40 μL of 1× TAE/Mg^{2+} buffer [to avoid self-lattice-formation of D(I,0)]. The sample test tube was then cooled gradually from 40 to 25 °C by placing the sample in 2 L of water in a Styrofoam box to facilitate further hybridization. The final concentration of each sample was 100 nM (Figure 2).

For a double-domain DNA lattice, equal amounts of annealed individual tiles of a given linear boundary were mixed in a new test tube. For example, 5 μL of RBRU and RBSU were added to 40 μL of 1× TAE/Mg^{2+} buffer for B(I,II). The sample test tube was then cooled gradually from 40 to 25 °C by placing the sample in 2 L of water in a Styrofoam box to facilitate further hybridization (the second annealing step). The final concentration of B(I,II) was 100 nM. Finally, 5 μL of annealed individual tiles [D(I,1) without the D(I,1)-4 strand for ON(I), and DR(II,0) and DS(II,0) for OFF(II)], 5 μL of 1 μM D(I,1)-4, and 10 μL of annealed boundary B(I,II) were added together into a new test tube containing 20 μL of 1× TAE/Mg^{2+} buffer. In the third annealing step, the sample test tube was cooled slowly from 30 to 25 °C by placing the sample in 2 L of water in a Styrofoam box. Final concentrations of the boundary and the two patterns were 20 and 100 nM, respectively (Figure 3).

For a quadruple-domain DNA lattice, the annealed seed tile and equal amounts of the annealed boundary tiles of a given cross boundary were mixed in a new test tube. For example, 2 μL of SR and 5 μL of RBRU and RBSU for B(I,II), LBRU, and LBSU for B(II,III), LBRD and LBSD for B(III,IV), and RBRD

https://doi.org/10.1021/acsomega.2c02556
ACS Omega 2022, 7, 26514−26522

and RBSD for B(I,IV) were added to 8 μL of 1× TAE/Mg^{2+} buffer for B(I,II,III,IV,S). The sample test tube was then cooled gradually from 40 to 25 °C by placing the sample in 2 L of water in a Styrofoam box to facilitate further hybridization (the second annealing step). The final concentrations of the seed and individual linear boundaries were 40 and 100 nM, respectively. Finally, 5 μL of annealed individual tiles [D(I,0) without the D(I,0)-4 strand for OFF(I), DR(II,1) and DS(II,0) for ST(II), D(III,0) without the D(III,0)-4 strand for OFF(III), and DR(IV,1) and DS(IV,1) for ON(IV)], D(I,0)-4, D(III,0)-4, and 10 μL of annealed boundary B(I,II,III,IV,S) were added together into a new test tube. In the third annealing step, the sample test tube was cooled slowly from 30 to 25 °C by placing the sample in 2 L of water in a Styrofoam box. The final concentrations of seed, boundaries, and patterns were 8, 20, and 100 nM, respectively (Figure 4).

AFM Imaging. Onto a 5 × 5 mm^2 cleaved mica substrate was deposited 40 μL of 1× TAE/Mg^{2+} buffer. Then, 2 μL of an annealed sample was pipetted onto the mica, and an additional 20 μL of 1× TAE/Mg^{2+} buffer was dispensed on an oxide-sharpened silicon nitride AFM tip (Veeco Inc., CA, USA). AFM images were obtained on a Digital Instruments Nanoscope III (Veeco Inc., CA, USA) in the scan-assist mode with a multimode fluid cell head (Figures 2–4).

■ ASSOCIATED CONTENT

Supporting Information

The Supporting Information is available free of charge at https://pubs.acs.org/doi/10.1021/acsomega.2c02556.

Sequence designs of seed, boundary, and unit tiles for the generation of different patterns in a single lattice; detailed sticky end assignment of the seed, boundary, and unit tiles for each domain; list of tiles with corresponding strands; names of sticky ends and corresponding DNA base sequences; DNA base sequence of all strands used in the multi-domain patterns; and AFM images of double-domain and quadruple-domain lattices without overlaid guidelines (PDF)

■ AUTHOR INFORMATION

Corresponding Author

Sung Ha Park − *Department of Physics and Sungkyunkwan Advanced Institute of Nanotechnology (SAINT), Sungkyunkwan University, Suwon 16419, Republic of Korea;* orcid.org/0000-0002-0256-3363; Email: sunghapark@skku.edu

Authors

Soojin Jo − *Department of Physics and Sungkyunkwan Advanced Institute of Nanotechnology (SAINT) and Institute of Basic Science, Sungkyunkwan University, Suwon 16419, Republic of Korea*

Sungjin Lee − *Department of Physics and Sungkyunkwan Advanced Institute of Nanotechnology (SAINT) and Institute of Basic Science, Sungkyunkwan University, Suwon 16419, Republic of Korea*

Suyoun Park − *Department of Physics and Sungkyunkwan Advanced Institute of Nanotechnology (SAINT) and Institute of Basic Science, Sungkyunkwan University, Suwon 16419, Republic of Korea*

Anshula Tandon − *Department of Physics and Sungkyunkwan Advanced Institute of Nanotechnology (SAINT) and Institute of Basic Science, Sungkyunkwan University, Suwon 16419, Republic of Korea*

Thi Bich Ngoc Nguyen − *Department of Physics and Sungkyunkwan Advanced Institute of Nanotechnology (SAINT), Sungkyunkwan University, Suwon 16419, Republic of Korea*

Thi Hong Nhung Vu − *Department of Physics and Sungkyunkwan Advanced Institute of Nanotechnology (SAINT), Sungkyunkwan University, Suwon 16419, Republic of Korea*

Muhammad Tayyab Raza − *Department of Physics and Sungkyunkwan Advanced Institute of Nanotechnology (SAINT), Sungkyunkwan University, Suwon 16419, Republic of Korea*

Complete contact information is available at: https://pubs.acs.org/10.1021/acsomega.2c02556

Author Contributions

[§]S.J. and S.L. equally contributed to this work.

Funding

This work was supported by the National Research Foundation (NRF) of Korea (2019R1I1A1A01060208, 2020R1I1A1A01055405, 2021R1A2C1005279, and 2022R1A2C1004386).

Notes

The authors declare no competing financial interest.

■ REFERENCES

(1) Watson, J. D.; Crick, F. H. C. Molecular Structure of Nucleic Acids: A Structure for Deoxyribose Nucleic Acid. *Nature* **1953**, *171*, 737−738.

(2) Seeman, N. C. Nucleic acid junctions and lattices. *J. Theor. Biol.* **1982**, *99*, 237−247.

(3) Rothemund, P. W. K.; Ekani-Nkodo, A.; Papadakis, N.; Kumar, A.; Fygenson, D. K.; Winfree, E. Design and characterization of programmable DNA nanotubes. *J. Am. Chem. Soc.* **2004**, *126*, 16344−16352.

(4) Fujibayashi, K.; Murata, S. Precise simulation model for DNA tile self-assembly. *IEEE Trans. Nanotechnol.* **2009**, *8*, 361−368.

(5) Seeman, N. C. DNA in a material world. *Nature* **2003**, *421*, 427−431.

(6) Wei, B.; Dai, M.; Yin, P. Complex shapes self-assembled from single-stranded DNA tiles. *Nature* **2012**, *485*, 623−626.

(7) Rothemund, P. W. K. Folding DNA to create nanoscale shapes and patterns. *Nature* **2006**, *440*, 297−302.

(8) Seeman, N. C.; Sleiman, H. F. DNA nanotechnology. *Nat. Rev. Mater.* **2018**, *3*, 17068.

(9) Ke, Y.; Ong, L. L.; Shih, W. M.; Yin, P. Three-dimensional structures self-assembled from DNA bricks. *Science* **2012**, *338*, 1177−1183.

(10) Yin, P.; Hariadi, R. F.; Sahu, S.; Choi, H. M. T.; Park, S. H.; LaBean, T. H.; Reif, J. H. Programming DNA tube circumferences. *Science* **2008**, *321*, 824−826.

(11) He, Y.; Chen, Y.; Liu, H.; Ribbe, A. E.; Mao, C. Self-assembly of hexagonal DNA two-dimensional (2D) arrays. *J. Am. Chem. Soc.* **2005**, *127*, 12202−12203.

(12) Fu, T. J.; Seeman, N. C. DNA double-crossover molecules. *Biochemistry* **1993**, *32*, 3211−3220.

(13) Shin, J.; Kim, J.; Amin, R.; Kim, S.; Kwon, Y. H.; Park, S. H. Artificial DNA lattice fabrication by noncomplementarity and geometrical incompatibility. *ACS Nano* **2011**, *5*, 5175−5179.

(14) He, Y.; Tian, Y.; Ribbe, A. E.; Mao, C. Highly connected two-dimensional crystals of DNA six-point-stars. *J. Am. Chem. Soc.* **2006**, *128*, 15978−15979.
(15) Hamada, S.; Murata, S. Substrate-assisted assembly of interconnected single-duplex DNA nanostructures. *Angew. Chem., Int. Ed.* **2009**, *48*, 6820−6823.
(16) Kim, B.; Amin, R.; Lee, J.; Yun, K.; Park, S. H. Growth and restoration of a T-tile-based 1D DNA nanotrack. *Chem. Commun.* **2011**, *47*, 11053−11055.
(17) Winfree, E.; Liu, F.; Wenzler, L. A.; Seeman, N. C. Design and self-assembly of two-dimensional DNA crystals. *Nature* **1998**, *394*, 539−544.
(18) Schulman, R.; Winfree, E. Synthesis of crystals with a programmable kinetic barrier to nucleation. *Proc. Natl. Acad. Sci. U.S.A.* **2007**, *104*, 15236−15241.
(19) Park, S. H.; Yin, P.; Liu, Y.; Reif, J. H.; LaBean, T. H.; Yan, H. Programmable DNA self-assemblies for nanoscale organization of ligands and proteins. *Nano Lett.* **2005**, *5*, 729−733.
(20) Wang, H. Proving theorems by pattern recognition−II. *Bell Syst. Tech. J.* **1961**, *40*, 1−41.
(21) Zhang, C.; Su, M.; He, Y.; Zhao, X.; Fang, P.; Ribbe, A. E.; Jiang, W.; Mao, C. Conformational flexibility facilitates self-assembly of complex DNA nanostructures. *Proc. Natl. Acad. Sci. U.S.A.* **2008**, *105*, 10665−10669.
(22) Mao, C.; LaBean, T. H.; Reif, J. H.; Seeman, N. C. Logical computation using algorithmic self-assembly of DNA triple-crossover molecules. *Nature* **2000**, *407*, 493−496.
(23) Barish, R. D.; Rothemund, P. W. K.; Winfree, E. Two computational primitives for algorithmic self-assembly: copying and counting. *Nano Lett.* **2005**, *5*, 2586−2592.
(24) Fujibayashi, K.; Hariadi, R.; Park, S. H.; Winfree, E.; Murata, S. Toward reliable algorithmic self-assembly of DNA tiles: a fixed-width cellular automaton pattern. *Nano Lett.* **2007**, *8*, 1791−1797.
(25) Cho, H.; Mitta, S. B.; Song, Y.; Son, J.; Park, S.; Ha, T. H.; Park, S. H. 3-input/1-output logic implementation demonstrated by DNA algorithmic self-assembly. *ACS Nano* **2018**, *12*, 4369−4377.
(26) Raza, M. T.; Tandon, A.; Park, S.; Lee, S.; Nguyen, T. B. N.; Vu, T. H. N.; Jo, S.; Nam, Y.; Jeon, S.; Jeong, J. H.; Park, S. H. Demonstration of elementary functions via DNA algorithmic self-assembly. *Nanoscale* **2021**, *13*, 19376−19384.
(27) Park, S.; Tandon, A.; Cho, H. J.; Raza, M. T.; Lee, S. J.; Chopade, P.; Ha, T. H.; Park, S. H. Ternary representation of N (N= 1 or 2)-input and 1-output algorithmic self-assembly demonstrated by DNA. *Nanotechnology* **2019**, *31*, 085604.
(28) Tandon, A.; Song, Y.; Mitta, S. B.; Yoo, S.; Park, S.; Lee, S.; Raza, M. T.; Ha, T. H.; Park, S. H. Demonstration of Arithmetic Calculations by DNA Tile-Based Algorithmic Self-Assembly. *ACS Nano* **2020**, *14*, 5260−5267.
(29) Clever, G. H.; Kaul, C.; Carell, T. DNA-Metal Base Pairs. *Angew. Chem., Int. Ed.* **2007**, *46*, 6226−6236.
(30) Douglas, S. M.; Bachelet, I.; Church, G. M. A logic-gated nanorobot for targeted transport of molecular payloads. *Science* **2012**, *335*, 831−834.
(31) Selmi, D. N.; Adamson, R. J.; Attrill, H.; Goddard, A. D.; Gilbert, R. J.; Watts, A.; Turberfield, A. J. DNA-templated protein arrays for single-molecule imaging. *Nano Lett.* **2011**, *11*, 657−660.
(32) Edwardson, T. G.; Lau, K. L.; Bousmail, D.; Serpell, C. J.; Sleiman, H. F. Transfer of molecular recognition information from DNA nanostructures to gold nanoparticles. *Nat. Chem.* **2016**, *8*, 162−170.
(33) Hsi-Yang Fritz, M.; Leinonen, R.; Cochrane, G.; Birney, E. Efficient storage of high throughput DNA sequencing data using reference-based compression. *Genome Res.* **2011**, *21*, 734−740.
(34) Ceze, L.; Nivala, J.; Strauss, K. Molecular digital data storage using DNA. *Nat. Rev. Genet.* **2019**, *20*, 456−466.
(35) Matange, K.; Tuck, J. M.; Keung, A. J. DNA stability: a central design consideration for DNA data storage systems. *Nat. Commun.* **2021**, *12*, 1358.
(36) Lin, C.; Liu, Y.; Rinker, S.; Yan, H. DNA tile based self-assembly: building complex nanoarchitectures. *Chemphyschem* **2006**, *7*, 1641−1647.
(37) Tandon, A.; Kim, S.; Song, Y.; Cho, H.; Bashar, S.; Shin, J.; Ha, T. H.; Park, S. H. Calculation of π and Classification of Self-avoiding Lattices via DNA Configuration. *Sci. Rep.* **2019**, *9*, 2252.
(38) Luo, J.; Zhang, W.; Su, J.; Xiang, F. Hexagonal Convolutional Neural Networks for Hexagonal Grids. *IEEE Access* **2019**, *7*, 142738−142749.
(39) Wüthrich, C. A.; Stucki, P. An algorithmic comparison between square- and hexagonal-based grids. *CVGIP Graph. Models Image Process.* **1991**, *53*, 324−339.

https://doi.org/10.1021/acsomega.2c02556
ACS Omega 2022, 7, 26514−26522